IPEM
Institute of Physics and
Engineering in Medicine

PAPER • OPEN ACCESS

X-ray diffraction from bone employing annular and semi-annular beams

View the article online for updates and enhancements.

X-ray diffraction from bone employing annular and semi-annular beams

A J Dicken[1], **J P O Evans**[1], **K D Rogers**[2], **N Stone**[3], **C Greenwood**[2], **S X Godber**[4], **D Prokopiou**[2], **J G Clement**[5], **I D Lyburn**[6], **R M Martin**[7] **and P Zioupos**[2]

[1] Imaging Science Group, Nottingham Trent University, Nottingham, UK
[2] Cranfield Forensic Institute, Cranfield University, Shrivenham, UK
[3] Physics and Astronomy, University of Exeter, Exeter, UK
[4] Halo X-ray Technologies Ltd, Nottingham, UK
[5] Melbourne Dental School, University of Melbourne, Melbourne, Australia
[6] Medical Imaging Department, Cobalt Health, Cheltenham, UK
[7] School of Social and Community Medicine, University of Bristol, Bristol, UK

E-mail: paul.evans@ntu.ac.uk

CrossMark

Abstract

There is a compelling need for accurate, low cost diagnostics to identify osteo-tissues that are associated with a high risk of fracture within an individual. To satisfy this requirement the quantification of bone characteristics such as 'bone quality' need to exceed that provided currently by densitometry. Bone mineral chemistry and microstructure can be determined from coherent x-ray scatter signatures of bone specimens. Therefore, if these signatures can be measured, *in vivo*, to an appropriate accuracy it should be possible by extending terms within a fracture risk model to improve fracture risk prediction.

In this preliminary study we present an examination of a new x-ray diffraction technique that employs hollow annular and semi-annular beams to measure aspects of 'bone quality'. We present diffractograms obtained with our approach from *ex vivo* bone specimens at Mo Kα and W Kα energies. Primary data is parameterized to provide estimates of bone characteristics and to indicate the precision with which these can be determined.

Keywords: x-ray diffraction, diagnostics, osteoporosis, annular beam

(Some figures may appear in colour only in the online journal)

1. Introduction

Osteoporosis is a debilitating condition that has a significant social, health and economic impact the world over. It is a contributing factor in more than 1.5 million fractures per annum in the US (National Osteoporosis Foundation 2002a) and while it can occur at any age it is most common in the elderly, particularly postmenopausal women (National Osteoporosis Foundation 2002b). Osteoporosis is characterized by low bone mass and the structural deterioration of tissue, which inevitably leads to bone fragility and an increased susceptibility to fracture (Sastry *et al* 2007). Given the population scale of the condition, low cost and accurate diagnosis is highly desirable. Currently the principal diagnostic tool is dual-energy x-ray absorptiometry (DEXA) which estimates bone mineral density (BMD) (Small 2005). BMD has been shown to be correlated with bone strength and fracture risk. However, BMD is not a sufficient predictor of whole bone mechanical properties (Boskey 2002). It has been shown that $\approx 30\%$ of the variation in compressive strength of bone cannot be attributed to mineral density (Ammann and Rizzoli 2003). Boskey (2002) suggests that other physico-chemical properties of bone mineral (commonly referred to as 'bone quality' (Kohles and Martinex 200)) such as crystal size, chemistry and 'perfection' must also be taken into consideration when predicting bone strength (Boskey 2002, 2003) (although the precise relationships between such factors and bone strength remain elusive). This argument is supported elsewhere in the literature. For example, several studies have reported changes to carbonate content concentration of bone apatite upon aging and therapy (Miller *et al* 2001, Huang *et al* 2003). Further, changes in crystallite size and/or perfection with age have also been noted by some authors, though there is some conflict as to whether crystallite size and/or perfection increases (Grynpas 1993, Boskey 2002, 2003, Gourian-Arsiquaud *et al* 2009, Boskey 2010) or decreases (Sastry *et al* 2007) with age. This difference in opinion is perhaps unsurprising given the small number of *ex vivo* specimens (Boskey 2003, Gourian-Arsiquaud *et al* 2009) that have been examined. Differences in sample storage conditions and preparation can also contribute significantly to differences in sample microstructure (McElderry *et al* 2011). For example, contact with water is known to result in significant dissolution of bone nanocrystals (Rey *et al* 2009). Chemicals such as formalin, which are often used for fixation (Scarano *et al* 2003, Ohman *et al* 2008, Unger *et al* 2010), have also been found to influence the mechanical properties of bone depending on the fixation time (Wilke *et al* 2011) (i.e. they can become harder (Van Haaren *et al* 2008)).

X-ray diffraction (XRD) is able to determine simultaneously several aspects of 'bone quality' (Boskey 2002) and has been used extensively to study bone mineral crystal microstructure. This technique is conducted typically in reflection mode at relatively soft x-ray energies i.e. Cu Kα, ≈ 8 keV to optimize the magnitude and angular distribution of the coherent scatter. However, photons with this energy have a limited penetrating capability e.g. $40\,\mu$m of hydroxyapatite is sufficient to absorb 95% of these photons. Thus as an *in vivo* diagnostic probe this approach is unsuitable due to its potentially high doses and low signal strength. Recently Almer and Stock (2005) and Stock *et al* (2008) have successfully demonstrated x-ray diffraction signatures from bone at significantly greater x-ray energies ≈ 80.7 keV by employing a synchrotron source. Synchrotron sources mitigate against the relatively low scattering cross section of bone mineral by providing significantly greater intensity. However, synchrotrons are impractical for the widespread implementation of a cost effective diagnostic tool.

Consequently, there is a need to determine the crystal microstructural properties of bone mineral *in vivo* using readily accessible technologies. To this end we have been considering a new approach to obtain coherent scatter data. The principles of an alternative XRD technique termed focal construct geometry (FCG) employing an annular beam have recently been

investigated elsewhere (Evans *et al* 2010, Rogers *et al* 2010). This technique can be realised at low cost and can increase diffraction intensities by a factor of >20. Some studies have also been undertaken at more diagnostically relevant x-ray energies (Dicken *et al* 2015) e.g. 58.4 keV. The preliminary study presented here demonstrates the first x-ray diffraction patterns obtained from bone using soft (i.e. Mo Kα) and hard (i.e. W Kα) x-ray implementations of FCG.

2. Methods

2.1. Theory background

Focal construct geometry (FCG) has been described in detail elsewhere (Evans *et al* 2010, Rogers *et al* 2010). To summarize, FCG is a transmission diffraction technique that employs an annular interrogating beam of radiation. When this beam is incident normally upon a poly or semi-crystalline material a continuum of Debye cones is produced from around a circular footprint at characteristic angles following Bragg's law, $n\lambda = 2d\sin\theta$. As these Debye cones propagate away from the sample they intersect to form relatively high intensity patterns or caustics in the diffracted flux. The caustics can be measured normal to the annular beam symmetry axis as concentric circular intensity fluctuations or as a series of condensation points, referred to as focal spots, distributed along the symmetry axis.

The preferred method of measuring FCG scattering signatures is by moving a point detector along the principal axis to establish diffraction intensities as a function of linear distance (see figure 1(a)). Providing that $2\theta > \varphi$ then each continuum or 2θ family of Debye cones forms a 'focused' spot on the z-axis. These spots can be measured and converted into a 1D diffractogram (see figure 1(b)) using equation:

$$2\theta = \tan^{-1}\left(\frac{Z_S \tan \phi}{Z_D - Z_S}\right) + \varphi \tag{1}$$

where Z_S is the source-to-sample distance, Z_D the source-to-detector distance and φ the half-opening angle of the interrogating annular beam. The most diagnostically relevant planes in hydroxyapatite are in the range 1.5–3.5 Å, (27.3º–11.6º 2θ/ Mo Kα). This method of data collection is most appropriate when $2\theta \gg \varphi$ because it permits a complete high intensity diffraction pattern to be collected by employing a relatively short linear translation of the detector along the z-axis.

Increasing the energy of the interrogating x-ray beam increases its penetrating capability but also decreases the angular resolution achievable with a detector of a given spatial resolution. The diagnostically relevant 2θ range for hydroxyapatite at W Kα is 7.98–3.42º. Therefore, collecting the FCG signatures through linear translation of a point detector (described in section 2.2) is not possible as the diffracted flux does not converge to form a spot (i.e. $2\theta < \varphi$). Similarly, when 2θ only slightly exceeds φ, the resultant diffraction spot is formed at an impractically large stand-off distance.

As an alternative the scattered flux from FCG can be measured by considering the caustic patterns (see figure 2(a)) normal to the annular beam symmetry axis. Providing that the detector is positioned such that the caustics are intercepted pre or post their corresponding axial focal spot positions then the relationship between a radius, r, on the detector and 2θ is well understood and given by:

$$2\theta = \tan^{-1}\left[\frac{Z_S \tan \varphi \pm r}{Z_D - Z_S}\right] + \varphi \tag{2}$$
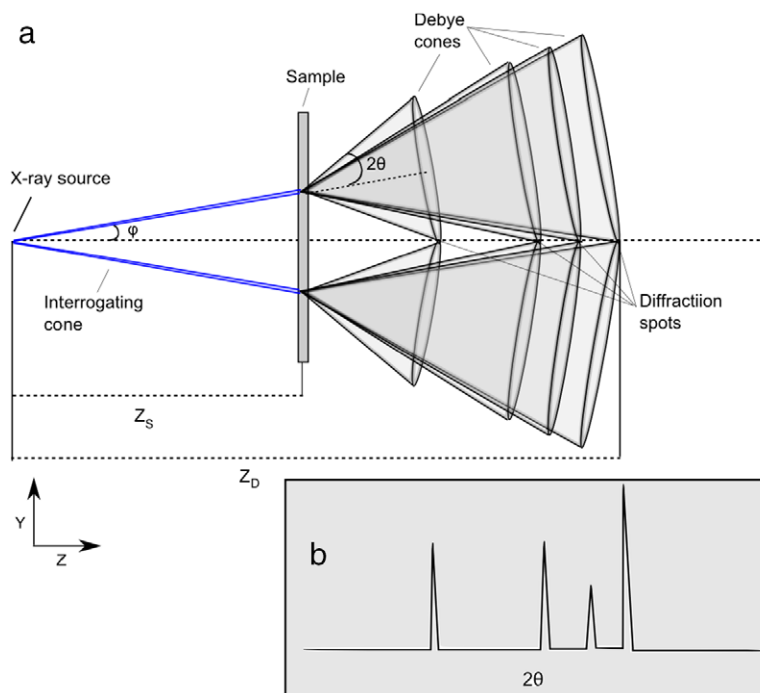
Figure 1. Schematic diagram of focal construct technology (a) and an example diffractogram (b). An annular beam is incident on a planar polycrystalline sample at distance Z_S. Debye cones are produced at every point of intersection for every d-spacing (four are shown) producing diffraction spots at different focal points along the principal axis.

where $-r$ and r accommodate pre and post diffraction spot conditions. However, this scenario for a 'full annular' beam presents an ill-posed problem as a caustic pattern of constant size r can be produced by incident diffracted flux at two different diffraction angles (given that the relative sample position is known). Also, hydroxyapatite contains many high order reflections that make positioning the detector in front of all the potential diffraction spot positions impractical from simple geometric considerations. In previous work we have employed annular beam XRD tomography [Evans *et al* 2014] to disambiguate superimposed caustics and identify unknown crystalline phases distributed at unknown positions within an inspection volume. Instead, in this paper we have adopted the use of a semi-annular beam (see figure 2(a)) to enable a static or 'staring mode' of signal collection. In this approach the beam asymmetry enables the sign of r to be encoded according to whether the caustic is detected within the interior half-field defined by the semi-annular beam or alternatively its mirror image (defined by the absence of the beam) $-r$ and r, respectively, as shown in figure 2(b).

At high energies there is a significant increase in inelastic scattering and thus balance filters (Jupp *et al* 2000, Beath and Cunningham 2009) were employed to produce a pseudo-monochromatic diffraction image.

2.2. Sample materials

Ex vivo bone specimens were considered appropriate for experimentation as the purpose of this study was to demonstrate proof of principle. Bovine cortical bone was obtained from the
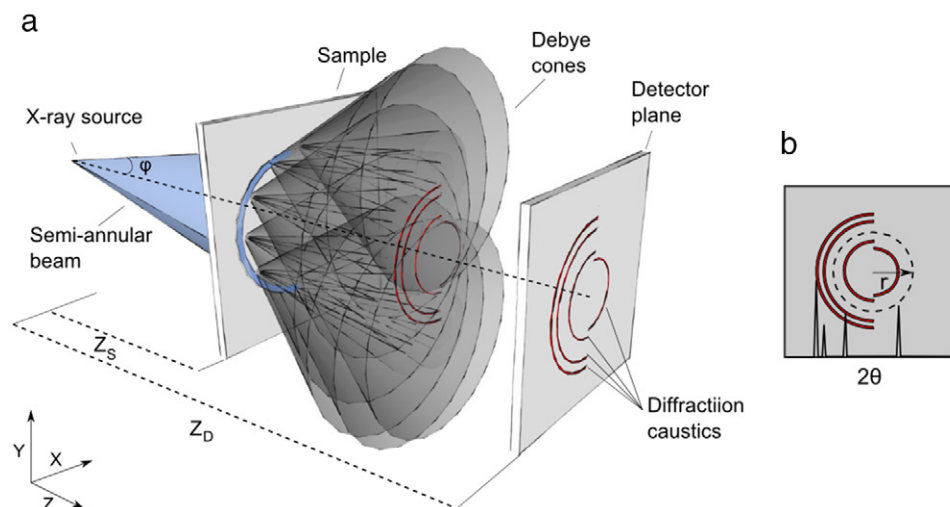
Figure 2. Schematic diagram of focal construct geometry employing a semi-annular beam (a) and an example caustic diffraction image (b). High intensity caustic patterns (one per d-spacing) form normal to the annular beam symmetry axis (Z) at radius r on the detector.

femoral neck. Bone specimens were cut to size using a Draper (B5355A) 14" band saw whilst frozen (to minimize friction between bone and band saw) and then allowed to thaw at room temperature. Soft tissue was removed using a scalpel as the samples were subsequently examined by other analytical techniques. The specimens used for the low energy experiments were ~2.5 mm thick and the annular beam was ~20.1 mm diameter at the specimen. The specimens used for the high energy experiments were ~10 mm thick and the semi-annular beam was ~22.5 mm diameter at its widest. The specimen thicknesses were limited by the penetrating ability of the relevant x-ray beam. Ultimately, diagnostically relevant thicknesses are envisaged to be in the cm range.

2.3. Experiment conditions

Low energy experiments were conducted using a Zr filtered molybdenum target sealed x-ray tube operating at 40 kV, 30 mA. A hollow conical beam with an opening angle of 3.97° was used to interrogate the specimens. Images were captured on a 1024 × 1024 (13 μm) Photonics Science cooled (−40 °C) CCD detector with a Gadox phosphor screen. The detector was translated along the principal axis 160–265 mm from the x-ray source in 0.1 mm steps. A bespoke sample holder was used to support the bone specimens at 150 mm from the x-ray source. Each frame was integrated for 7 s. Conventional diffractograms were created by integrating the signal from a 20 × 20 pixel area at the detector centre for each detector position and then converted into 2θ using equation (1).

The high energy experiments were conducted using a Hamamatsu microfocus x-ray source with a tungsten target and focal spot size of 40 μm; the accelerating voltage and current were 130 kV, 300 μA, respectively. A semi-annular beam with a half-opening angle of 3.98° was produced using a bespoke tungsten optic and lead absorption plate. Scattered x-rays were detected using a stationary 4 in diameter x-ray image intensifier incorporating a 0.5 mm aluminium window and a caesium iodide phosphor with terbium doped gadolinium oxysulphide
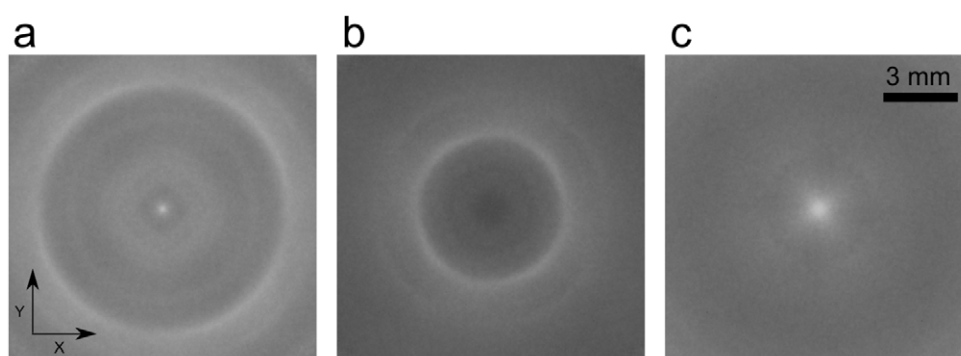
Figure 3. Low energy FCG images from bone captured at 173.9, 184.8 and 200.2 mm Z_D for images (a)–(c), respectively.

(G_2O_2S:Tb) phosphor screen, which was optically coupled to a 1280×1024 ($6.45\,\mu m$ pitch) 12 bit Peltier cooled CCD camera. The detector was placed 512 mm from the x-ray source. Rare earth metals filters 0.1 mm thick (i.e. Tm K-edge 59.39 keV and Er K-edge 57.49) were used sequentially and the resultant images were subtracted. The specimens were placed 162 mm from the x-ray source. Each frame was integrated for 20 s. Conventional diffractograms were created by radial integration following background subtraction and Savitzky–Golay smoothing. Reference patterns for each sample were collected on a Bruker D8 diffractometer operating in reflection mode ≈8 keV Cu kα. Comparisons between the FCG and conventional patterns are presented in section 3.

3. Results and discussion

Low energy 2D FCG images are illustrated in figure 3 for three different sample-to-detector distances. Although the FCG diffractogram can be collected by the linear translation of a point detector (described in section 2.2) the 2D detector images help to illustrate both the high intensity circular caustic patterns as well as the 'focused' diffraction maxima that form at the centre of the detector plane.

A typical low energy FCG diffractogram from a bone specimen obtained by integrating a 0.26×0.26 mm area on the 2D detector at the centre of the annular interrogating beam for each detector position is illustrated in figure 4. This is compared to a diffractogram of a bone sample obtained from a conventional diffractometer to act as a reference standard. Good correspondence can be seen between the peak positions, shapes and relative intensities (intensities have been normalized).

The reference standard data consists of a series of overlapping Bragg maxima at peak positions dictated by the crystallographic symmetry and lattice parameters for the calcium hydroxyapatite like bone mineral phase. The peaks are significantly broader than expected for a well crystallized polycrystalline phase due to the microstructural characteristics of the apatite e.g. nano-sized crystallites and microstrain. Lattice parameters are an indication of crystal chemistry (e.g. amount of CO_3 substitution) and peak broadening in excess of inherent instrumental broadening can indicate the average domain size of the crystallites.

The Bragg maxima recorded by FCG in transmission mode are significantly broader than those observed from the reference standard (obtained in reflection mode). This broadening is primarily attributed to geometric unsharpness due to the relatively large gauge volume (or
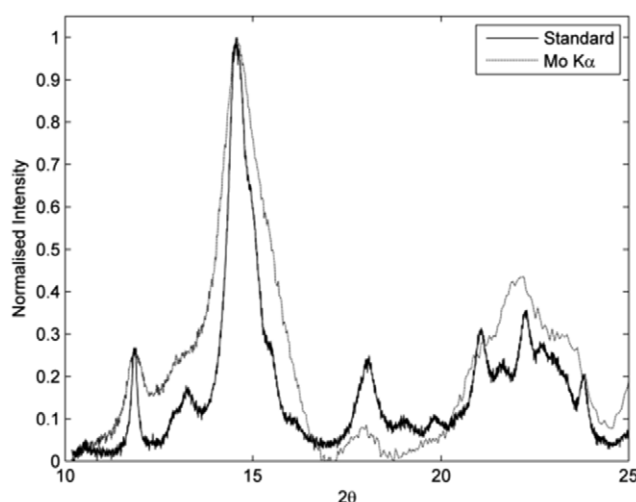
Figure 4. Comparison between diffractograms obtained from bone with low energy FCG in transmission mode and industry standard diffractometer operating in reflection mode.

extended specimen path) employed by FCG i.e. mm penetration as opposed micron penetration with the 'standard' diffractometer operating at Cu Kα wavelengths. A detailed analysis of this broadening phenomenon can be found elsewhere (Dicken *et al* 2015). Deconvolving this inherent instrument width from the observed data enables determination of the microstructural parameter values (Rogers *et al* 2012). Figure 5 illustrates an FCG diffractogram from a bone sample obtained by the high energy method described in section 2.3. The reference diffractogram is also shown.

As with the low energy data, the Bragg maxima positions between the high energy FCG diffractogram and the reference standard are consistent. Similarly to the previous arrangement the Bragg maxima obtained by FCG appear noticeably broader than those of the reference. However, this is anticipated given the FCG method interrogates a specimen two orders of magnitude thicker than that from the conventional apparatus.

The diffractograms from each experiment were parameterised using a full pattern fitting approach as follows. The approximate scattering angle, $2\theta_i$, of each diffraction maxima was calculated using Bragg's law, radiation wavelength and the lattice parameters for a calcium hydroxyapatite NIST standard (SRM 2910). The initial calculated diffractogram was produced from Pearson VII peak profiles centred at each $2\theta_i$ (other than at maxima positions that were systematically absent due to crystallographic symmetry). A non-linear least squares approach was then employed to minimise the calculated-observed residue by refining the individual peak areas, background (2nd order Chebychev polynomial), lattice parameters, and peak shapes (full width at half maximum). The resultant parameters are compared to those from a standard for calcium hydroxyapatite recorded by the International Centre for Diffraction Data (ICDD) and summarized within table 1.

Parameter values from the standard diffractometer are different to those from the ICDD standard primarily due to differences in chemistry between the bone bio-apatite and that of the geological apatite reported by ICDD. For example, substitution of 1 wt% PO_4 by CO_3 causes a reduction in 'a' by ~6 pm. Unit cell parameter values from the low energy FCG regime are not significantly different to those from the standard diffractometer data although the precision
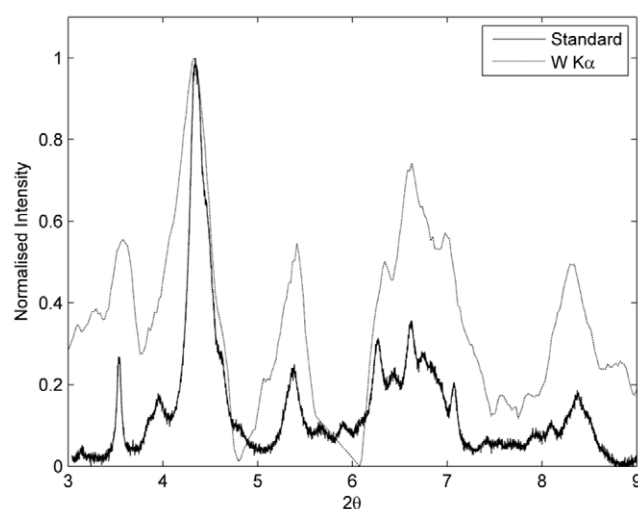
Figure 5. Comparison between a diffractogram obtained from bone employing pseudo-monochromatic high energy FCG diffraction in transmission mode against that of an industry standard diffractometer operating in reflection mode. A four frame average was taken for each rare earth filter.

Table 1. Summary of the unit cell lattice parameters derived from each of the experimental regimes. The errors are estimated standard deviations associated with the least squares fit precision.

	a(Å)	σ(a)	c(Å)	σ(c)	Cell volume (Å³)	σ(vol)
ICDD	9.432	—	6.881	—	530.139	—
Std. diffractometer	9.4176	0.0008	6.8824	0.0008	528.6	0.1
Low energy FCG	9.443	0.015	6.936	0.008	535.7	1.9
High energy FCG	9.315	0.008	6.882	0.004	517.1	1.0

is significantly compromised. This situation was expected due to the increase in geometric instrument broadening when employing FCG. In the broadening regime demonstrated by FCG applied to bone, our ability to determine lattice parameters (i.e. the % precision error in 'a' and 'c') decreases approximately linearly with diffraction peak broadening. For example, an increase in the FWHM of the 002 reflection results in an increase in the % error in 'c' by a factor of 3. However, in the context of deriving diagnostic information from the diffraction data, even doubling the 002 peak width would not compromise the determination of lattice parameters to the third decimal place and thus the data would remain significant. The high energy FCG data shows a lower value for 'a' although the precision is improved compared to that of the corresponding low energy data.

The coherent scattering cross section decreases with increasing energy. Consequently the ratio of the coherent scattering cross sections for tungsten Kα to molybdenum Kα is ~0.17 for cortical bone. Contrastingly the differences in scan time for the experiment results presented here are ~46:1 in favour of the high energy method rather than the low energy method. Such time savings, in part, demonstrate the advantages of using a 2D detector rather than sequential 1D measurement.

4. Conclusion

We have demonstrated two new implementations of FCG that can obtain diffraction patterns in transmission from bone samples. The diffractogram from the low energy FCG method (described in section 2.2) compares well with that from a conventional diffractometer. However, the lack of penetrating ability and the time overhead associated with sequential 1D measurement renders this approach impractical as a diagnostic tool. Increasing the characteristic x-ray energy from Mo Kα to W Kα facilitates greater penetrating capability but the concomitant reduction in diffraction scatter angle renders the use of FCG by sampling diffraction focal maxima problematic. We have found a semi-annular beam approach coupled with measuring high intensity diffraction caustics normal to the principal axis to be an effective solution. Pseudo-monochromising the beam using balance filtering has also mitigated against the decrease in coherent to incoherent scattering cross section ratio encountered at higher energies. Measuring the diffraction pattern in 2D rather than sequential 1D measurements also has the benefit of decreasing the measurement time by a factor of 46.

The data presented illustrates how, albeit at an early development stage, FCG derived lattice parameters can be measured to a precision that enables useful chemical information to be deduced. In the data presented, carbonate substitution into the apatite lattice can be measured to ~2 wt%. Although this is only one parameter that can be derived from the diffraction data, there is some evidence that it can be associated with the reduced bone quality in osteoporosis (Huang *et al* 2003) and thus be of clinical value in fracture risk prediction.

Although this is a preliminary study and the exposure times are, as yet, diagnostically inappropriate, it is hoped that this work will form the basis for a technique based on FCG to perform time critical high fidelity measurements of bone quality *in vivo*. Pseudo-monochromising the beam through balance filtering is an inherently wasteful process particularly for such a photon starved environment. Future developments will focus on increasing efficiency by employing energy resolving detectors where appropriate.

References

Almer J D and Stock S R 2005 Internal strains and stresses measured in cortical bone via high-energy x-ray diffraction *J. Struct. Biol.* **152** 14–27

Ammann P and Rizzoli R 2003 Bone strength and its determinants *Osteoporos. Int.* **14** 13–8 (PMID: 12730800)

Beath S R and Cunningham I A 2009 Pseudomonoenergetic x-ray diffraction measurements using balanced filters for coherent-scatter computed tomography *Med. Phys.* **36** 1839–47

Boskey A L 2002 Variations in bone mineral properties with age and disease *J. Musculoskelet. Neutronal Interact.* **2** 532–4

Boskey A 2003 Bone mineral crystal size *Osteoporos. Int.* **14** 16–21

Boskey A L and Coleman R 2010 Aging and bone *J. Dent. Res.* **89** 1333–48

Dicken A, Shevchuk A, Rogers K, Godber S and Evans P 2015 High energy transmission annular beam x-ray diffraction *Opt. Express* **23** 6304–12

Evans P, Rogers K, Chan J, Rogers J and Dicken A 2010 High intensity x-ray diffraction in transmission mode employing an analog of Poisson's spot *Appl. Phys. Lett.* **97** 204101

Evans P, Rogers K, Dicken A, Godber S and Prokopiou D 2014 X-ray diffraction tomography employing an annular beam *Opt. Express* **22** 11930–44

Gourian-Arsiquaud S, Burket J C, Havill L M, DiCarlo E, Doty S B, Mendelsohn R, Van der Meullen M C H and Boskey A L 2009 Spatial variation in osteonal bone properties relative to tissue in animal age *J. Bone Miner. Res.* **24** 1271–81

Grynpas M 1993 Age and disease-related changes in the mineral of bone *Calcif. Tissue Int.* **53** 57–64

Huang R Y, Miller L M, Carlson C S and Chance M R 2003 Characterization of bone mineral composition in the proximal tibia of Cynmolgus monkeys: effect of ovariectomy and nandrolone decanoate treatment *Bone* **30** 492–7

Jupp I D, Durrant P T, Ramsden D, Carte T, Dermody G, Pleasants I B and Burrows D 2000 The non-invasive inspection of Baggage using coherent x-ray scattering *Proc. IEEE Trans. Nucl. Sci.* **47** 1987–94

Kohles S S and Martinex D A 2000 Elastic and physicochemical relationships within cortical bone *J. Biomed. Mater. Res.* **49** 479–88

McElderry J, Kole M and Morris M 2011 Repeated freeze—thawing of bone tissue affects Raman bone quality measurements *J. Biomed. Opt.* **16** 071407

Miller L M, Vairavamurthy V, Chance M R, Mendelsohn R, Paschalis E P, Betts F and Boskey A L 2001 *In situ* analysis of mineral content and crystallinity in bone using infrared micro-spectroscopy of the v_4 PO_4^{3-} vibration *Biochim. Biophys. Acta* **1527** 11–9

National Osteoporosis Foundation 2002a *Physicians Guide to Prevention to Osteoporosis* (Washington, DC: National Osteoporosis Foundation)

National Osteoporosis Foundation 2002b *America's Bone Health: The State of Osteoporosis and Low Bone Mass in Our Nation* (Washington, DC: National Osteoporosis Foundation)

Ohman C, Dall'Ara E, Baleani M, Jan S and Viceonti M 2008 The effects of embalming using a 4% formalin solution on the compressive mechanical properties of human cortical bone *Clin. Biomech.* **23** 1294–8

Rey C, Combes C, Drouet C and Glimcher M J 2009 Bone mineral: update on chemical composition and structure *Osteoporos. Int.* **20** 1013–21

Rogers K, Evans P, Prokopiou D, Dicken A, Godber S and Rogers J 2012 Fundamental parameters approach applied to focal construct geometry for x-ray diffraction *Nucl. Instrum. Methods* A **690** 1–6

Rogers K, Evans P, Rogers J, Chan J and Dicken A 2010 Focal construct geometry—a novel approach to the acquisition of diffraction data *J. Appl. Crystallogr.* **43** 264–8

Sastry T P, Chandrsekaran A, Sundaraseelan J, Ramasastry M and Sreedhar R 2007 Comparative study of some physico-chemical characteristics of osteoporotic and normal human femur heads *Clin. Biochem.* **40** 907–12

Scarano A, Iezzi G and Piattelli A 2003 Common fixatives in hard tissue histology *Handbook of Histology Methods for Bone and Cartilage* (Clifton, NJ: Humana) pp 159–65

Small R E 2005 Uses and limitations of bone mineral density measurements in the management of osteoporosis *Med. Gen. Med.* **7** 3

Stock S R, De Carlo F and Almer J D 2008 High energy x-ray scattering tomography applied to bone *J. Struct. Biol.* **161** 144–50

Unger S, Blauth M and Schmolez W 2010 Effects of three different preservation methods on the mechanical properties of human and bovine cortical bone *Bone* **47** 1048–53

Van Haaren E H, Van der Zwaard B C, Van der Veen A J, Heyligers I C, Wuisman P I J M and Smitt T H 2008 *Acta Orthop.* **79** 708–16

Wilke H, Werner K, Haussler K and Reinehr M 2011 Theil-fixation preserves the non-linear load deformation characteristic of spinal motion segments, but increase their flexibility *J. Mech. Behav. Biomed. Mater.* **4** 2133–7